CrossMark
click for updates

High-quality AlGaN epitaxial structures and realization of UVC vertical-cavity surface-emitting lasers

Zhongming Zheng[1], Yukun Wang[1], Jason Hoo[2], Shiping Guo[2*], Yang Mei[1], Hao Long[1], Leiying Ying[1], Zhiwei Zheng[1] and Baoping Zhang[1*]

ABSTRACT AlGaN-based vertical-cavity surface-emitting lasers (VCSELs) have garnered recent interest due to their superior material properties and device benefits. Nevertheless, AlGaN-based VCSELs are extremely difficult to realize due to numerous technical limitations associated with both material epitaxial growth and chip fabrication. This study fabricated a high-quality AlGaN multiple quantum wells (MQWs) structure using epitaxial lateral overgrowth and analyzed it using X-ray diffraction (XRD) and photoluminescence (PL) measurements. With an edge dislocation density (DD) of 10^9 cm^{-2}, XRD measurements reveal that the AlN template is nearly fully relaxed. The subsequent AlGaN/AlN superlattice (SL) layer is introduced to decrease the edge DD, and the edge DD in the MQWs is ~10^8 cm^{-2}. According to PL measurements, the internal quantum efficiency of the MQWs is as high as 62%, and radiative recombination dominated the emission of the MQWs at room temperature. Using these epitaxial wafers, ultraviolet radiation C (UVC) VCSELs were fabricated using various techniques, including laser lift-off (LLO) and chemical mechanical polishing (CMP). The crystallinity of the MQWs was unaffected by sapphire substrate removal using LLO. After removing the sapphire substrate using LLO and CMP, UVC surface-stimulated emission was observed in MQWs. AlGaN-based UVC VCSELs with lasing wavelengths of 275.91, 276.28, and 277.64 nm have been fabricated. The minimum threshold for UVC VCSELs is 0.79 MW cm^{-2}, which is a record low.

Keywords: AlGaN, vertical-cavity surface-emitting lasers, epitaxial lateral overgrowth, laser lift-off, UVC

INTRODUCTION

Since it was first proposed in 1977, the vertical-cavity surface-emitting laser (VCSEL) has attracted significant interest from both basic research and industry due to its advantages, which include on-wafer testing, single mode output, low cost, two-dimensional (2D) array capability, circular beam, small divergence, simple collimation, and small wavelength shift. GaAs-based VCSELs have been successfully implemented in various fields, including 3D imaging, laser radar, and optical commu-

nication. Compared with GaAs, group III nitrides have high-temperature tolerance, radiation resistance, high breakdown voltage, high thermal conductivity, and direct bandgap, varying continuously from 0.76 eV for InN [1] to 6.14 eV for AlN [1]. Therefore, they are suitable for fabricating ultraviolet (UV) and visible light-emitting devices, including VCSELs. With the development of III-nitride growth techniques, nitride VCSELs can be fabricated and have been realized in the wavelength range from 275.9 [2] to 565.7 nm [3]. Among them, electrically pumped VCSELs with lasing wavelength above 400 nm have been demonstrated. Lu et al. [4] created the first electrically pumped GaN-based VCSEL at 462.8 nm and 77 K in 2008. Since then, the performance of electrically pumped GaN-based VCSELs has been significantly enhanced. A blue GaN-based VCSEL with 16 mW of output power [5] and a 2D 16 × 16 GaN-based VCSEL array with 1.19 W of output power [6] have been demonstrated. For green VCSELs, room temperature (RT) CW lasing was demonstrated using InGaN quantum dots. However, VCSELs with lasing wavelengths below 400 nm are all optically pumped, and only one has been reported in ultraviolet radiation B (UVB) (280–320 nm) [7] and ultraviolet radiation C (UVC) (200–280 nm) [2].

UV (deep UV) VCSELs can be used for material curing, photolithography, sterilization, the treatment of skin diseases, and solar-blind short-range communication. AlGaN multiple quantum wells (MQWs) structures frequently function as active layers in the UVB and UVC ranges. However, many technical challenges are still limitations to achieving AlGaN-based VCSELs, including material growth technique and device fabrication process. On the one hand, aluminum atoms have a high adhesion coefficient and a low surface migration velocity, resulting in a 3D island-like growth mode and an increase in the dislocation density (DD) in AlGaN epilayers [8]. On the other hand, crystalline quality, particularly DD, also influences internal quantum efficiency (IQE). It has been reported that as DD increases from 2×10^8 to 6×10^9 cm^{-2}, the IQE of AlGaN-based MQWs decreases from 64% to 4% [9]. On the other hand, AlGaN epilayers with low DD are difficult to grow, and the following strategies have been proposed to reduce DD in AlGaN epilayers: using high crystalline quality AlN as the template in the growth of AlGaN [8]; using nano-patterned sapphire

[1] Department of Electronic Engineering, Optoelectronics Engineering Research Center, School of Electronic Science and Engineering (National Model Microelectronics College), Xiamen University, Xiamen 361005, China
[2] Advanced Micro-Fabrication Equipment Inc., Shanghai 201201, China
* Corresponding authors (emails: shipingguo@amecnsh.com (Guo S); bzhang@xmu.edu.cn (Zhang B))

substrate (NPSS) to introduce epitaxial lateral overgrowth (ELOG) of AlN [10]; increasing the growth temperature to reduce the coalescence-related DD in AlN template [10]; inserting superlattice (SL) structure between the AlN template and AlGaN epilayer to further reduce DD in the AlGaN epilayer [8,11–13]. In addition, the quantum confined stark effect (QCSE) ascribed to the polarization of nitrides decreases the efficiency of radiative recombination and the IQE.

However, the fabrication of AlGaN-based VCSELs is also challenging. The optical absorption increases as the wavelength decrease, so nitride-distributed Bragg reflectors (DBRs) are incompatible with UV (deep UV) VCSELs. The structure of dielectric DBRs is then a viable option. The structure must eliminate the sapphire substrate of the AlGaN-based wafer. Laser lift-off (LLO) has been used to remove sapphire substrates from GaN-based wafers, where the decomposition of GaN is an important issue. The decomposition of an AlGaN layer on an AlGaN-based wafer is also crucial. Due to its high decomposition temperature and stable chemical properties, it is difficult to achieve the decomposition of AlGaN with a high Al content. By optimizing the "sacrificial layer" (GaN or AlGaN), laser energy, and laser spot size, we have removed the sapphire substrate of AlGaN wafers by LLO [2,14,15] and demonstrated a 275.9-nm optically pumped VCSEL with AlGaN-based MQWs structure [2]. LLO reveals the feasibility of separating large-area AlGaN epilayers from sapphire substrates.

In this study, the material quality and fabrication processes for UVC VCSELs were optimized further. Concerning the enhancement of AlGaN crystalline quality, ELOG of the AlN template was employed, and the epitaxial structure was improved. The results demonstrate that the AlN template is relaxed with a DD of $\sim 10^9$ cm^{-3} and that the AlGaN/AlN SL layer can effectively reduce the edge DD, resulting in 10^8 cm^{-3} for the MQWs. The IQE of the MQWs is as high as 62%. To further optimize the fabrication processes, chemical mechanical polishing (CMP) is used to remove the disordered layer generated on the sample after LLO. The clear observation of stimulated emission at 278.7 nm from the epilayers after LLO and CMP demonstrates that LLO does not degrade the crystalline quality of the MQWs. Finally, UVC VCSELs with the lowest threshold value ever reported were demonstrated.

EXPERIMENTAL SECTION

Growth of AlGaN epilayers
All epilayer structures were grown on a NPSS using an Advanced Micro-Fabrication Equipment Inc. China (AMEC) Prismo HiT3 metal-organic chemical vapor deposition (MOCVD) platform. The structure diagram of the as-grown epilayers is shown in Fig. 1a. A 4-μm AlN layer was grown on an NPSS utilizing ELOG. In addition, a 200-nm AlN/Al$_{0.6}$Ga$_{0.4}$N SL layer, a 1.2-μm n-Al$_{0.6}$Ga$_{0.4}$N layer, five pairs of Al$_{0.4}$Ga$_{0.6}$N (2 nm)/Al$_{0.5}$Ga$_{0.5}$N (6 nm) MQWs, and a 60-nm p-Al$_{0.6}$Ga$_{0.4}$N cladding layer were sequentially epitaxially grown on top of the AlN template. The n-Al$_{0.6}$Ga$_{0.4}$N and SL growth temperatures and pressures are 1100°C and 40 torr, respectively. The n-Al$_{0.6}$Ga$_{0.4}$N layer has a Si doping concentration of 8×10^{18} cm^{-3}.

Fabrication of UVC VCSELs
As depicted in Fig. 1b, UVC VCSELs were fabricated by first depositing the bottom HfO$_2$/SiO$_2$ DBR, followed by DBR patterning, sapphire substrate removal by LLO, thickness thinning and surface smoothing by CMP, and finally deposition of the top HfO$_2$/SiO$_2$ DBR. Due to the superior adhesion of the adhesive to the GaN surface, DBR patterning can increase the subsequent bonding strength. A 248-nm KrF excimer laser with 20-ns pulse duration and 1-Hz periodic frequency was used in the LLO procedure. Fig. 1b demonstrates the UVC VCSEL structure. To investigate additional optical and structural properties of the epitaxial structure after LLO, a structure denoted A and depicted in Fig. 2a was fabricated using LLO.

Measurements
X-ray diffraction (XRD) analysis was performed with Cu Kα line (λ = 1.5406 Å). Transmission electron microscopy (TEM), scanning electron microscopy (SEM), and atomic force microscopy (AFM) were used to analyze the morphology of the epilayers. Photoluminescence (PL) measurements and optical pumping were performed using a 240-nm laser with 5-ns pulse
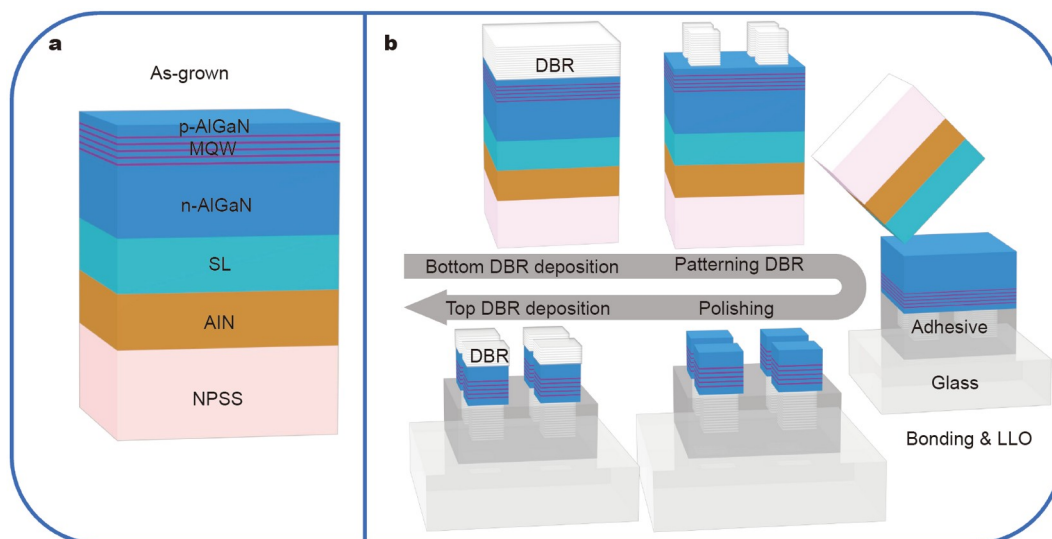
Figure 1 (a) Structure diagrams of the as-grown epilayers; (b) UVC VCSEL fabrication processes.
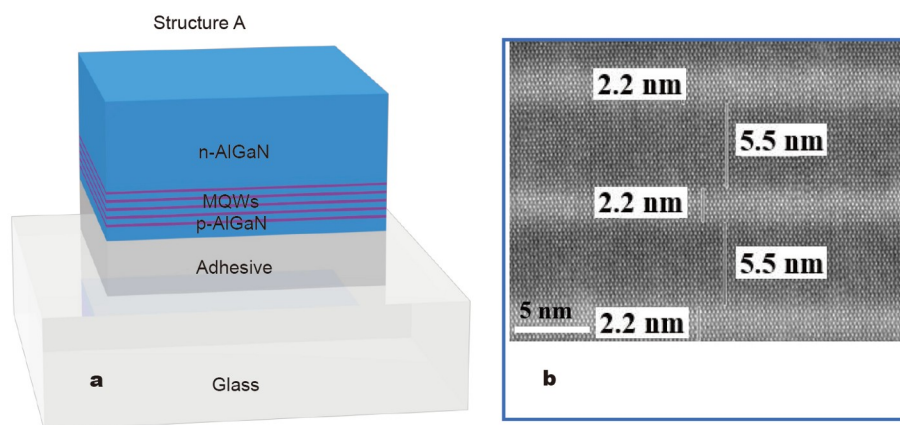
Figure 2 Structure A (a) and cross section TEM image of the MQWs (b).

duration and 20-Hz periodic frequency. A helium cycle cooling system was used in the temperature-dependent (TD) PL measurements.

RESULTS AND DISCUSSION

Structural and optical properties of the as-grown AlGaN epilayers
Fig. 2b shows the cross-sectional TEM image of the MQWs; clear boundaries between the well and barrier layers are observed, indicating a good crystalline quality of the MQWs. Fig. 3 shows the XRD patterns of the as-grown epilayers. Fig. 3a, b show (002) and (102) 2θ-ω scans of the epilayers, respectively. Diffraction peaks of AlN and n-$Al_{0.6}Ga_{0.4}N$ were observed, and lattice constants for the two layers were estimated, as listed in Table 1 (details see Section S1 in the Supplementary information). The lattice constants of the AlN template are close to the strain-free ones ($a = 0.3112$ nm and $c = 0.4982$ nm), indicating that the AlN template is almost fully relaxed. The a-lattice constant of the n-$Al_{0.6}Ga_{0.4}N$ layer is almost equal to that of the AlN template, suggesting that the n-$Al_{0.6}Ga_{0.4}N$ layer is fully strained. Screw and edge DDs in the AlN template and the n-$Al_{0.6}Ga_{0.4}N$ layer are also presented in Table 1. They are estimated from the full width of the half maximum (FWHM) of the (002) and (102) rocking curves of the two layers [16] (see Section S1 in the Supplementary information), as demonstrated in Fig. 3c–f, respectively. The screw DD in the two layers has the same order of magnitude. However, edge DD in the n-$Al_{0.6}Ga_{0.4}N$ layer is an order of magnitude lower than that in the AlN template, attributable to the reduction effect of AlN/ $Al_{0.6}Ga_{0.4}N$ SL on the DDs [8,11,12]. The DDs in the MQWs are approximately equal to that in the n-$Al_{0.6}Ga_{0.4}N$ layer, with the IQE expected to be 65%, according to Ref. [9].

Optical properties of the as-grown epilayers were measured by excitation power-dependent PL and TD PL, respectively, as shown in Fig. 4. The excitation power-dependent PL was performed at RT and 3.23 K, respectively. At RT, three interference peaks are observed at 271.00, 274.71, and 277.06 nm (Fig. 4a). According to the three peak positions, the structure's thickness is calculated to be 5.6 µm, close to the designed thickness of 5.5 µm. The emission point is located at 274.71 nm. As illustrated in Fig. 4b, the integral intensity varied linearly with excitation energy. Because of the low defect density in the active region, it indicates that radiative recombination predominated

in the emission during the measurement [17–19]. Because of the temperature effect on the bandgap, the emission center shifts to 271.19 nm at 3.23 K, as shown in Fig. 4c. As shown in Fig. 4d, the integral intensity decreased linearly as the excitation energy increased below 1 µJ. Nonetheless, when the excitation energy was greater than 1 µJ, the integral intensity varied sublinearly with an exponent of 0.68. When the excitation is greater than 1 µJ, Auger recombination dominates the emission, which is primarily caused by excess carrier injection into the active region.

The emission center of the as-grown epilayers shifts from 271 to 274 nm as the temperature increases from 3.23 to 300 K (RT), and three interference peaks are also observed at 271, 274 and 277 nm, as shown in Fig. 4e. As the temperature rises, the three peak positions become nearly constant, indicating that the thickness of the epitaxial structure remains constant during the measurement. Fig. 4f depicts the integral intensity as it varies with the reciprocal temperature. The activation energy of nonradiative channels can be obtained by fitting the data to the Arrhenius formula [20]. The two activation energies, E_a (4.8 meV) and E_b (72.3 meV), may correspond to point defect activation and exciton decomposition, respectively. The IQE of the MQWs can be calculated from the integral intensity ratio between RT and 3.23 K, assuming the IQE is 100% at 3.23 K. The estimated IQE is 62%, close to the XRD measurement value. When compared with reported research results, 85% [21], 69% [22], 50% [23], 55% [24], 43% [25], and 8% [26], it is a reasonably high value.

Design of UVC VCSEL
The fabrication of the UVC VCSEL began with the deposition of the bottom DBR and ended with the deposition of the top DBR. HfO_2 and SiO_2 are used to make DBRs because their extinction coefficients are lower than those of other transparent oxides, as shown in Table 2. At 276 nm, the reflectance of top and boom DBRs is calculated to be 95.3% and 97.7%, respectively. The calculated cavity reflective spectrum is shown in Fig. 5a. A single cavity mode is observed at 280.9 nm. Single-mode emission is beneficial for communications and other applications. The calculated optical field in a 2λ cavity is shown in Fig. 5b. The active region perfectly aligns with the field's antinode, which optimizes the optical confinement factor. In addition, the interface between the epilayer and the DBR is at the field node, which may
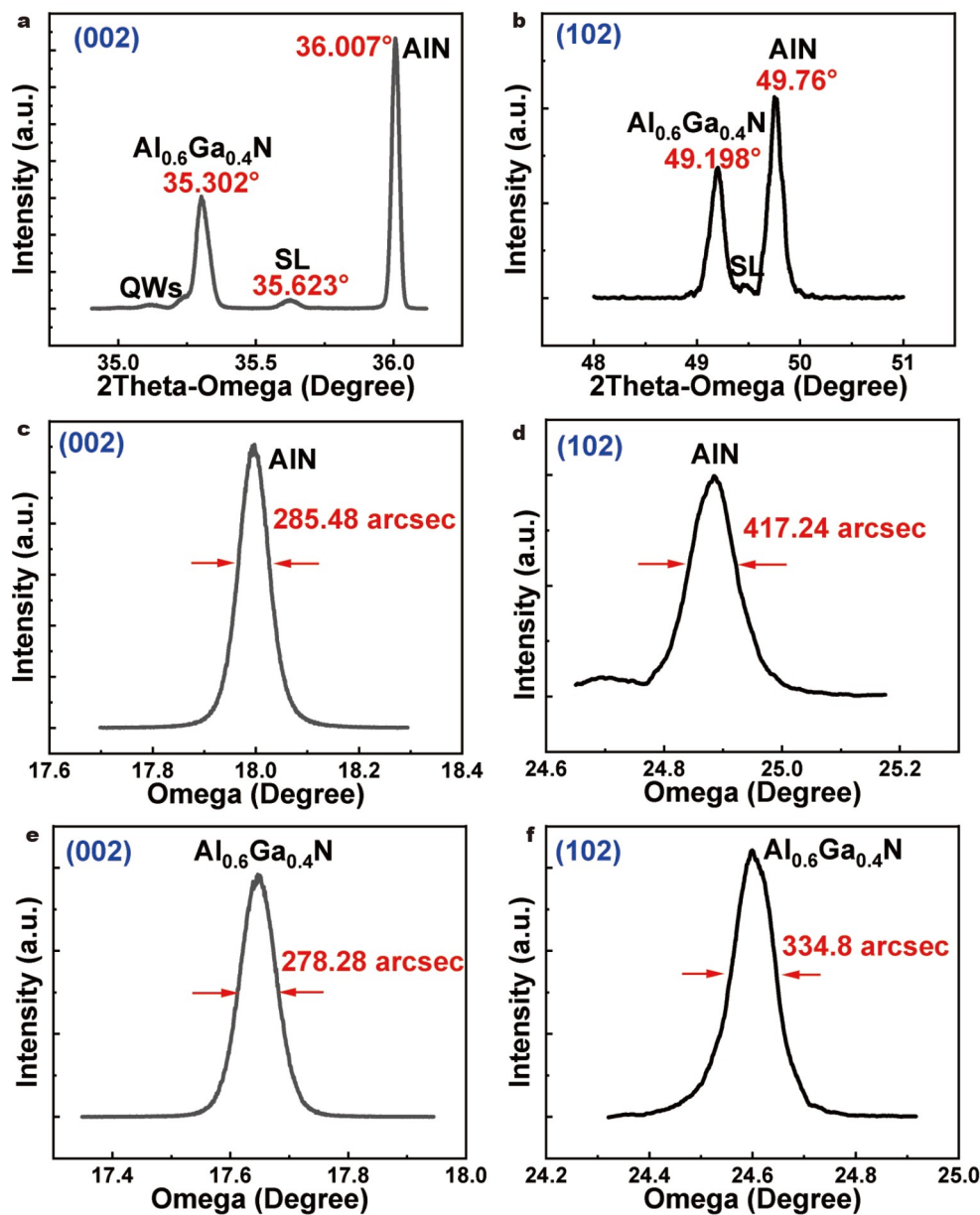
Figure 3 XRD patterns of the as-grown AlGaN epilayers: (a) (002) and (b) (102) 2θ-ω scan; (c) (002) and (d) (102) rocking curves of the AlN template; (e) (002) and (f) (102) rocking curves of the n-Al$_{0.6}$Ga$_{0.4}$N layer.

Table 1 XRD results of the AlN and n-Al$_{0.6}$Ga$_{0.4}$N layers

	AlN (as-grown)	Al$_{0.6}$Ga$_{0.4}$N (as-grown)	Al$_{0.6}$Ga$_{0.4}$N (after CMP)
a (nm)	0.3116	0.3119	0.3147
c (nm)	0.4985	0.5081	0.5038
Screw dislocation (cm^{-2})	1.77×10^{8}	1.62×10^{8}	3.37×10^{8}
Edge dislocation (cm^{-2})	1.57×10^{9}	1.06×10^{8}	2.03×10^{8}
FWHM $_{(002)\ \omega\text{-scan}}$ (arcsec)	285.48	278.28	397.62
FWHM $_{(102)\ \omega\text{-scan}}$ (arcsec)	417.24	334.80	320.08

reduce optical scattering loss [14].

LLO process in the UVC VCSEL fabrication

Removing the sapphire substrate by LLO is critical in the UVC VCSEL fabrication process. As a result, the dielectric DBR structure is realized. The optimized laser energy density for the AlGaN wafer is 3.7 J cm^{-2} pulse^{-1}. Fig. 6a, b show cross-sectional SEM images of the as-grown epilayers and structure A, respectively. After LLO, the epilayer thickness is 1.36 μm, corresponding to 1.2 μm n-Al$_{0.6}$Ga$_{0.4}$N, 40 nm MQWs, and 60 nm p-Al$_{0.6}$Ga$_{0.4}$N layers. The structural thickness variation before (6 μm) and after (1.36 μm) the LLO process indicates that the epilayers and sapphire substrate were separated at the interface between the SL and n-Al$_{0.6}$Ga$_{0.4}$N layers. Fig. 7a, b show XRD patterns of structure A, with a clear diffraction peak of the n-Al$_{0.6}$Ga$_{0.4}$N layer and no diffraction peaks of the SL or AlN layers. It implies that the SL and AlN layers were removed
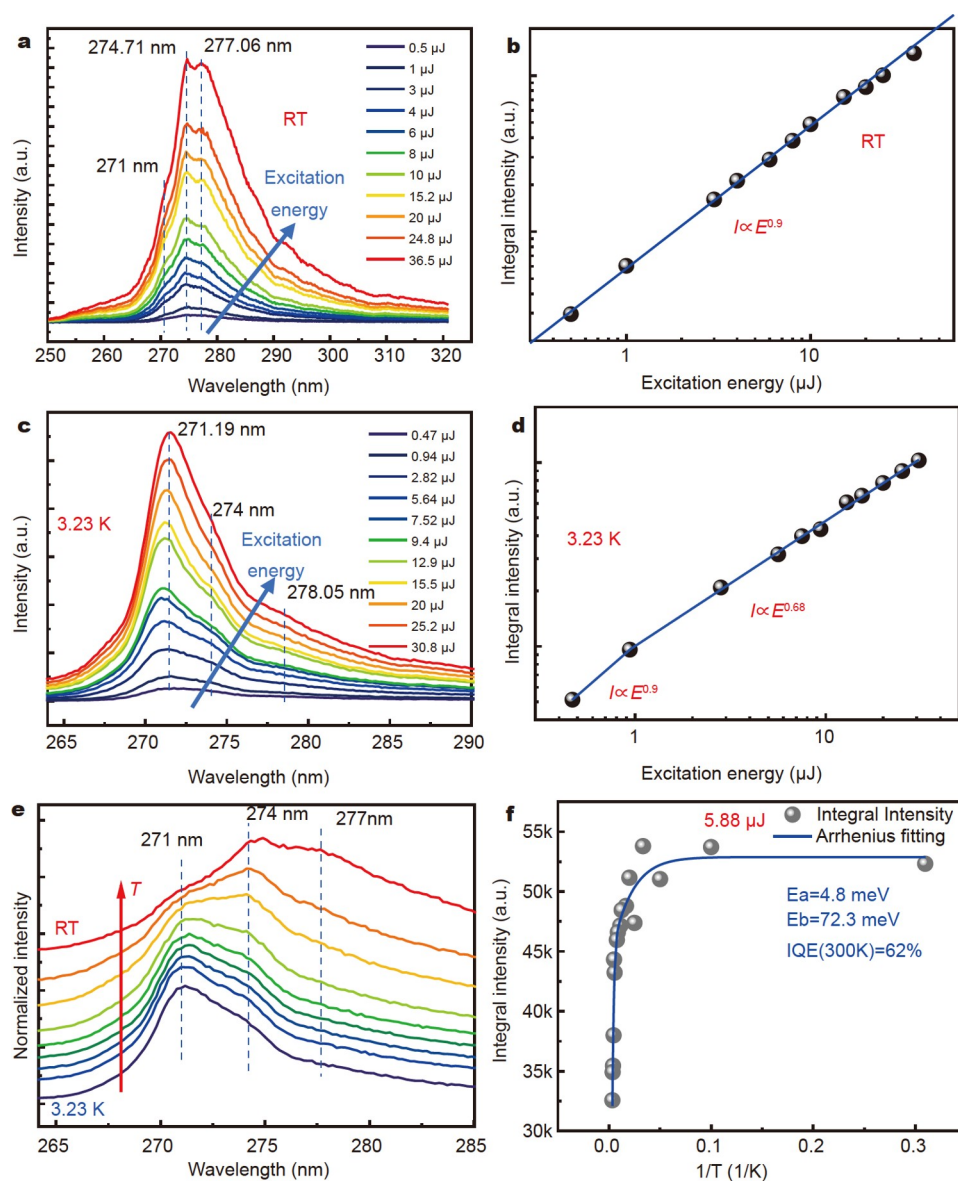
Figure 4 Spectra of the as-grown epilayers. Excitation power-dependent PL and the corresponding integral intensity *vs.* excitation energy in double logarithmic coordinates. (a, b) At RT; (c, d) at 3.23 K. Normalized spectra of TD PL (e) and the corresponding integral intensity *vs.* 1/*T* (f).

Table 2 Refractive indexes and extinction coefficients of transparent oxides

| Materials	Refractive index	Extinction coefficient
SiO_2 [27]	1.5	0
HfO_2	1.98	7.67×10^{-3}
Ti_3O_5 [28]	2.3	0.2
Ta_2O_5 [27]	2.4	0.2
TiO_2 [29]	2.8	1

during the LLO process, which is supported by the SEM results. The rocking curve's FWHM is 2376.1 arcsec, 8.5 times greater than that of the as-grown one. It is due to partial recrystallization of AlGaN at the n-$Al_{0.6}Ga_{0.4}N$ surface during the LLO process. The AlGaN layer was heated by the laser and consequently decomposed during the LLO process. Some products, including Al, Ga, and N_2, reacted at high temperatures, forming a disordered AlGaN layer that must be removed.

CMP process in the UVC VCSEL fabrication

CMP was used to remove the disordered layer and smooth the epilayer surface. Structure A has a thickness of 150 nm after CMP. As shown in Fig. 8, a small surface root-mean-square (RMS) roughness of 0.96 nm is obtained. A smooth surface is required to reduce optical scattering loss [14]. The XRD patterns of structure A after CMP are depicted in Fig. 7c–f, respectively. The n-$Al_{0.6}Ga_{0.4}N$ layer and the MQWs show diffraction peaks. Table 1 also includes screw and edge DDs in the n-$Al_{0.6}Ga_{0.4}N$ layer, as well as lattice constants in the n-$Al_{0.6}Ga_{0.4}N$ layer. Both screw and edge DDs are in the order of 10^8 cm^{-2}, indicating that the disordered layer is removed after the CMP process. The DDs, on the other hand, are greater than that of the as-grown epilayer. It is due to the inhomogeneous thickness of the epilayers following polishing. Different epilayer thicknesses correspond to different strain relaxations, which increases the FWHM. The presence of some of the disordered layers on the sample following CMP may increase the FWHM. The n-$Al_{0.6}$
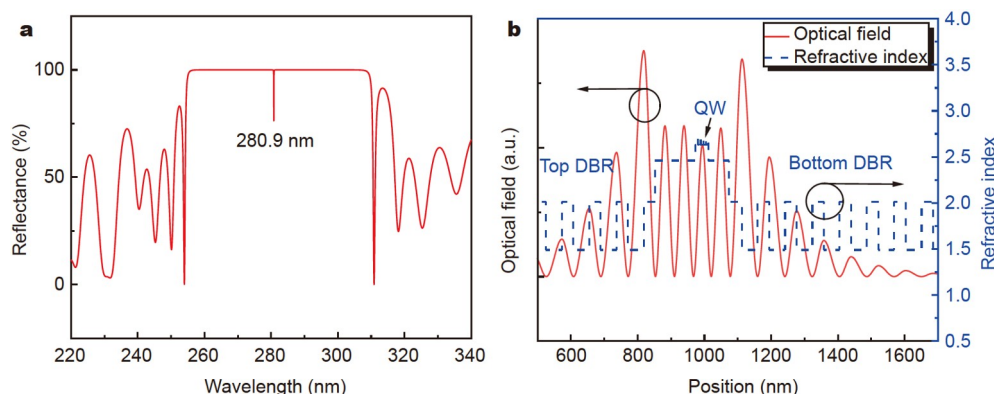
Figure 5 Calculated cavity reflective spectrum (a) and optical field inside the cavity (b).
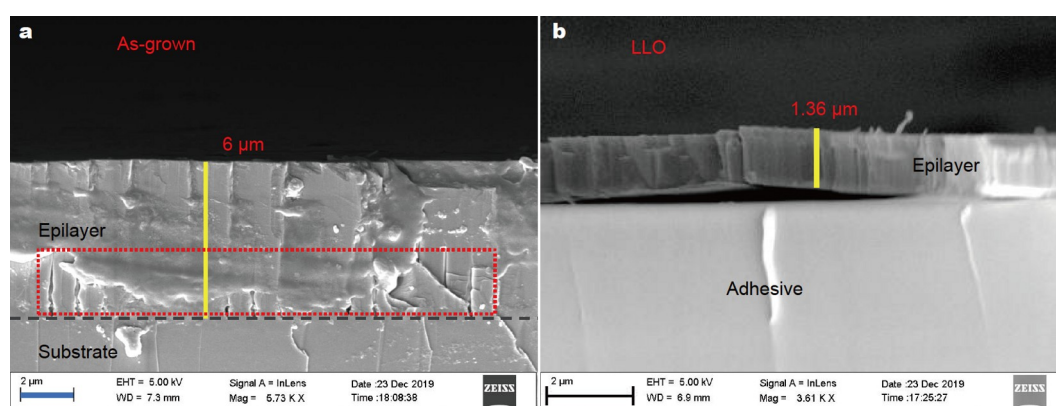
**Figure 6** Cross-sectional SEM images of the as-grown epilayers (a) and structure A before CMP (b).

Ga$_{0.4}$N layer exhibits a significant change in lattice constants. After CMP, the *a*-lattice constant of the n-Al$_{0.6}$Ga$_{0.4}$N layer in structure A equals the strain-free one (0.3146 nm, calculated from Vegard law [30]). It indicates that the n-Al$_{0.6}$Ga$_{0.4}$N layer relaxed during LLO. The *c*-lattice constant, on the other hand, is less than the strain-free constant (0.5063 nm). This effect is most likely caused by Si doping, which lowers the *c*-lattice constant [31].

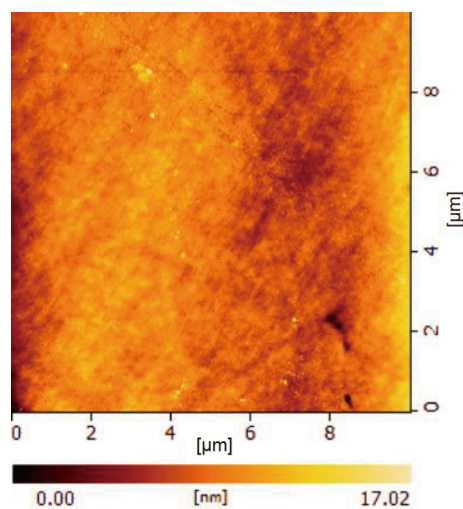**Optical properties of structure A after CMP**
The IQE of structure A after CMP was also calculated by computing the integral intensity ratio between RT and 3.23 K, yielding 65%, as shown in Fig. 9a. It is nearly identical to the as-grown one, indicating that the crystalline quality of the active region does not degrade after LLO and CMP. Excitation power-dependent PL at RT was used to measure the optical properties of structure A after CMP. With increased excitation power, a surface-stimulated emission peak with a linewidth of 3 nm appears at 278.7 nm, as shown in Fig. 9b, along with spontaneous emission with an FWHM of 12 nm. The corresponding integral intensity as a function of excitation power is also shown in Fig. 9c, and a clear kink point can be seen at 1.5 μJ pulse^{-1} when surface-stimulated emission becomes visible. The spectrum of structure A before stimulated emission is shown in the inset of Fig. 9b, and the emission peak was at 280 nm. It is worth noting that the emission position for the as-grown epilayers

shifts from 274.71 to 280 nm for structure A. The redshift of 85 meV could be due to differences in strain in the MQWs before and after the substrate was removed. The *a*-lattice of the barrier and well layers in as-grown epilayers (structure A) is equal to that of the AlN template (n-Al$_{0.6}$Ga$_{0.4}$N layer). The in-plane strain in the well layers is then calculated to be −1.41% before LLO and −0.52% after LLO. It modifies the well layers' polarization-related QCSE and bandgap. According to Refs. [32,33], the polarization-related built-in electric field of the well layers is 0.61 MV cm^{-1} before LLO and 0.70 MV cm^{-1} after LLO. The well layers' corresponding emission energy decreases by 0.18 meV [34], which is far less than the amount of redshift (see Section S2 in the Supplementary information). The nitride bandgap is reported to vary with strain, and the variation of the GaN bandgap with strain has been calculated [35]. Assuming that the well layers' bandgap variation with strain is similar to that of GaN, the bandgap of the well layers is estimated to decrease by 88.7 meV [35], which is close to the amount of redshift (see Section S3 in the Supplementary information). It implies that the redshift is primarily caused by bandgap variation.

The as-grown epilayers do not exhibit surface-stimulated emission. The "holes" in the epitaxial structure, as shown in the red rectangle in Fig. 6a, increase the optical scattering loss. These holes are caused by ELOG nitride on NPSS. It has also been reported in numerous publications [10,36,37]. Furthermore,
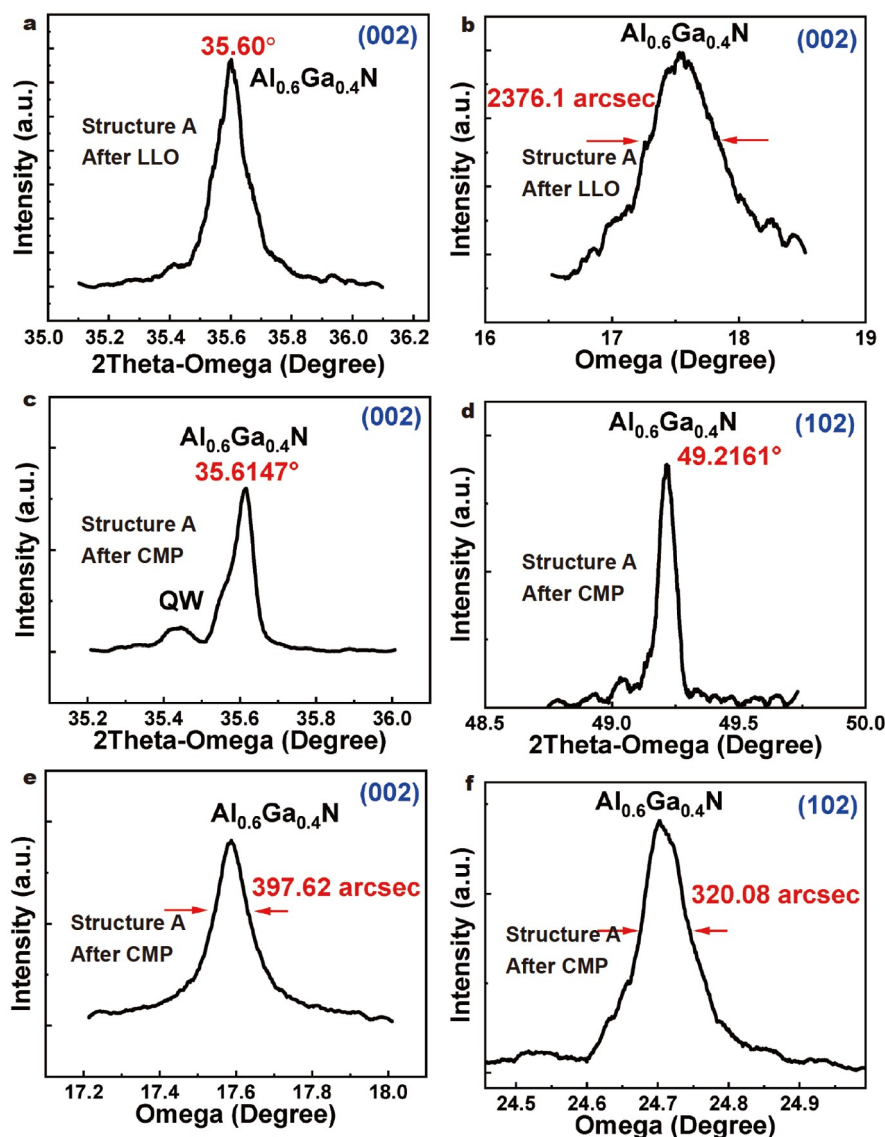
Figure 7 XRD patterns of $Al_{0.6}Ga_{0.4}N$ in structure A. (a) (002) 2θ-ω scan; (b) (002) rocking curve after LLO; (c) (002) and (d) (102) 2θ-ω scan after CMP; (e) (002) and (f) (102) rocking curves after CMP.


**Figure 8** AFM image of the surface of structure A after CMP.

high DD in the AlN template increases scattering loss. Structure A, conversely, has a thinner thickness and smoother surfaces after CMP. It reduces optical absorption loss and increases light resonance within epilayers. UVC surface stimulated emission at 260 nm from AlGaN MQWs epilayers was also reported by Li *et al.* [38]. The epitaxial structure was formed on a sapphire planar substrate. Light resonance benefits from smooth interfaces and surfaces in epitaxial structures.

Measurements of the UVC VCSELs

The optical pumping technique was used to characterize the optical properties of the UVC VCSELs. Fig. 10 depicts a series of lasing spectra obtained from various UVC VCSELs. The three VCSELs are designated as VCSEL-I, VCSEL-II [2], and VCSEL-III, and in that order, the lasing wavelengths are 277.64, 275.91, and 276.28 nm, respectively. The entire lasing is a single mode, which agrees with the cavity reflective spectrum. The corresponding threshold power density is 0.79, 1.21, and
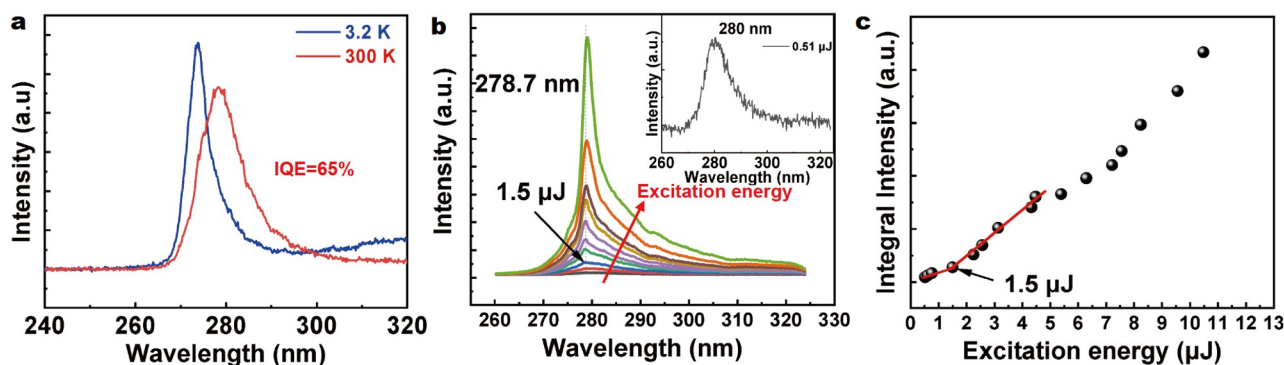
Figure 9 IQE measurement (a), surface stimulated emission spectra (b), and the corresponding integral emission intensity as a function of excitation power (c) of structure A after CMP.
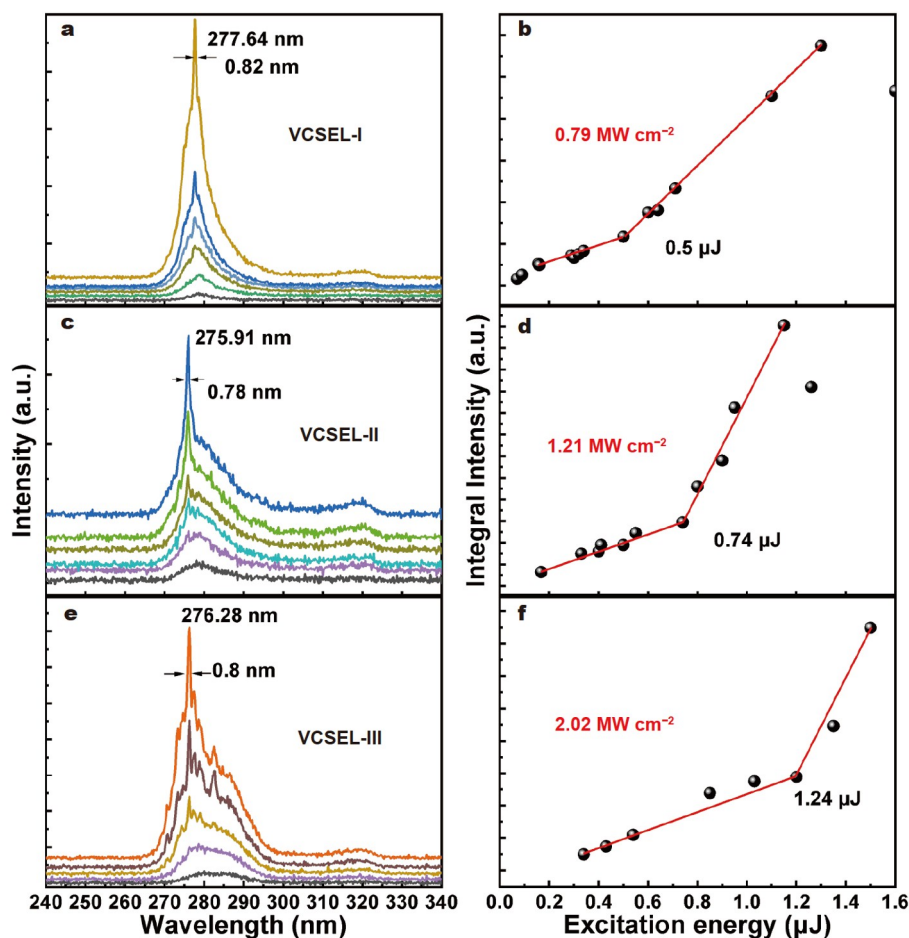
Figure 10 Lasing spectra and the corresponding integral emission intensity as a function of excitation energy. (a, b) VCSEL-I; (c, d) VCSEL-II; (e, f) VCSEL-III.

2.02 MW cm^{-2}, respectively. The linewidth is 0.8 nm. There are two possible explanations for the different thresholds. First, the detuning between the gain peak and the cavity mode position of three different VCSELs varies; the smaller the detuning, the smaller the threshold. The FWHM of the spontaneous emission of the three VCSELs at 0.3 J (before lasing) is 7.57, 10.81, and 15.61 nm, respectively. In general, the FWHM is related to the crystalline quality. The FWHM is increased by crystalline

dislocation, distortion, and defect. As a result, VCSEL-I is thought to have better crystalline quality, resulting in a lower lasing threshold.

Compared with other studies, this work demonstrated the early lasing of VCSEL in the UVC range, as well as a low threshold power density of 0.79 MW cm^{-2}, as shown in Fig. 11. It benefits from high IQE AlGaN MQWs with good crystalline quality. The key processes that do not degrade the crystalline
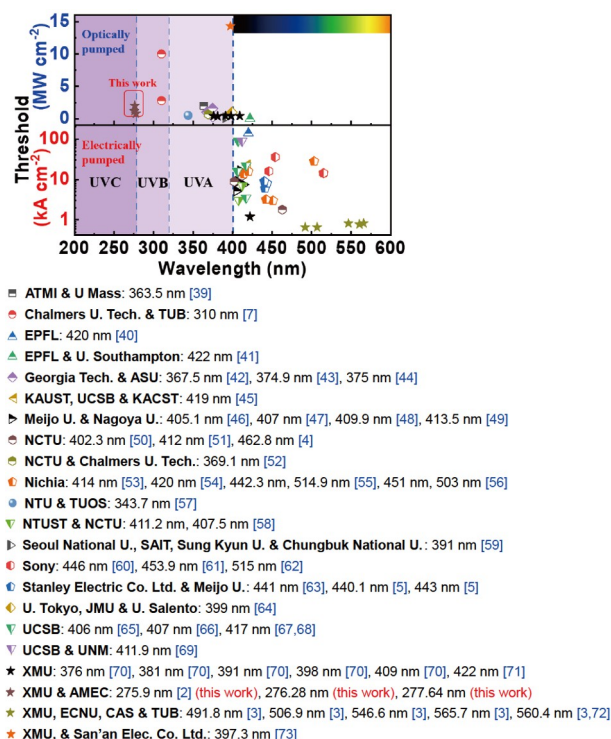
Figure 11 Progress of nitride VCSELs.

quality of the MQWs are LLO and CMP. The cavity design also improves optical confinement and decreases optical loss.

CONCLUSIONS

An ELOG AlGaN-based epitaxial structure was grown on NPSS. The XRD and PL measurements exhibited low screw and edge DDs in the MQWs of $\sim 10^8$ cm^{-2} with a high IQE of 62%. Our unique LLO process does not degrade the crystallinity of the AlGaN MQWs, and UVC surface stimulated emission is achieved from structure A after CMP. AlGaN-based VCSELs with lasing at 275.91, 276.28, and 277.64 nm are successfully demonstrated.

1 Vurgaftman I, Meyer JR. Band parameters for nitrogen-containing semiconductors. J Appl Phys, 2003, 94: 3675–3696

2 Zheng Z, Mei Y, Long H, et al. AlGaN-based deep ultraviolet vertical-cavity surface-emitting laser. IEEE Electron Device Lett, 2021, 42: 375–378

3 Mei Y, Weng GE, Zhang BP, et al. Quantum dot vertical-cavity surface-emitting lasers covering the 'green gap'. Light Sci Appl, 2016, 6: e16199

4 Lu TC, Kao CC, Kuo HC, et al. CW lasing of current injection blue GaN-based vertical cavity surface emitting laser. Appl Phys Lett, 2008, 92: 141102

5 Kuramoto M, Kobayashi S, Akagi T, et al. High-output-power and high-temperature operation of blue GaN-based vertical-cavity surface-emitting laser. Appl Phys Express, 2018, 11: 112101

6 Kuramoto M, Kobayashi S, Akagi T, et al. Watt-class blue vertical-cavity surface-emitting laser arrays. Appl Phys Express, 2019, 12: 091004

7 Hjort F, Enslin J, Cobet M, et al. A 310 nm optically pumped AlGaN vertical-cavity surface-emitting laser. ACS Photonics, 2021, 8: 135–141

8 Li D, Jiang K, Sun X, et al. AlGaN photonics: Recent advances in materials and ultraviolet devices. Adv Opt Photon, 2018, 10: 43–110

9 Ban K, Yamamoto J, Takeda K, et al. Internal quantum efficiency of whole-composition-range AlGaN multiquantum wells. Appl Phys Express, 2011, 4: 052101

10 Jain R, Sun W, Yang J, et al. Migration enhanced lateral epitaxial overgrowth of AlN and AlGaN for high reliability deep ultraviolet light emitting diodes. Appl Phys Lett, 2008, 93: 051113

11 Wang HM, Zhang JP, Chen CQ, et al. AlN/AlGaN superlattices as dislocation filter for low-threading-dislocation thick AlGaN layers on sapphire. Appl Phys Lett, 2002, 81: 604–606

12 Zhang JP, Wang HM, Gaevski ME, et al. Crack-free thick AlGaN grown on sapphire using AlN/AlGaN superlattices for strain management. Appl Phys Lett, 2002, 80: 3542–3544

13 Sun WH, Zhang JP, Yang JW, et al. Fine structure of AlN/AlGaN superlattice grown by pulsed atomic-layer epitaxy for dislocation filtering. Appl Phys Lett, 2005, 87: 211915

14 Zheng Z, Li Y, Paul O, et al. Loss analysis in nitride deep ultraviolet planar cavity. J Nanophoton, 2018, 12: 1

15 Zheng Z, Long H, Matta S, et al. Photoassisted chemical smoothing of AlGaN surface after laser lift-off. J Vac Sci Tech B, 2020, 38: 042207

16 Moram MA, Vickers ME. X-ray diffraction of III-nitrides. Rep Prog Phys, 2009, 72: 036502

17 Mártil I, Redondo E, Ojeda A. Influence of defects on the electrical and optical characteristics of blue light-emitting diodes based on III–V nitrides. J Appl Phys, 1997, 81: 2442–2444

18 Wang H, Ji Z, Qu S, et al. Influence of excitation power and temperature on photoluminescence in InGaN/GaN multiple quantum wells. Opt Express, 2012, 20: 3932–3940

19 Xu RB, Xu H, Mei Y, et al. Emission dynamics of GaN-based blue resonant-cavity light-emitting diodes. J Lumin, 2019, 216: 116717

20 Yasan A, McClintock R, Mayes K, et al. Photoluminescence study of AlGaN-based 280 nm ultraviolet light-emitting diodes. Appl Phys Lett, 2003, 83: 4083–4085

21 Wang TY, Tasi CT, Lin CF, et al. 85% internal quantum efficiency of 280-nm AlGaN multiple quantum wells by defect engineering. Sci Rep, 2017, 7: 14422

22 Banal RG, Funato M, Kawakami Y. Extremely high internal quantum efficiencies from AlGaN/AlN quantum wells emitting in the deep ultraviolet spectral region. Appl Phys Lett, 2011, 99: 011902

23 Bhattacharyya A, Moustakas TD, Zhou L, et al. Deep ultraviolet emitting AlGaN quantum wells with high internal quantum efficiency. Appl Phys Lett, 2009, 94: 181907

24 Shatalov M, Sun W, Lunev A, et al. AlGaN deep-ultraviolet light-emitting diodes with external quantum efficiency above 10%. Appl Phys Express, 2012, 5: 082101

25 Dong P, Yan J, Zhang Y, et al. AlGaN-based deep ultraviolet light-emitting diodes grown on nano-patterned sapphire substrates with significant improvement in internal quantum efficiency. J Cryst Growth, 2014, 395: 9–13

26 Zeng J, Li W, Yan J, et al. Temperature-dependent emission shift and carrier dynamics in deep ultraviolet AlGaN/AlGaN quantum wells. Phys Status Solidi RRL, 2013, 7: 297–300

27 Rodríguez-de Marcos LV, Larruquert JI, Méndez JA, et al. Self-consistent optical constants of SiO$_2$ and Ta$_2$O$_5$ films. Opt Mater Express, 2016, 6: 3622–3637

28 Hakoe F, Tokoro H, Ohkoshi S. Dielectric and optical constants of λ-Ti$_3$O$_5$ film measured by spectroscopic ellipsometry. Mater Lett, 2017, 188: 8–12

29 Kruchinin VN, Perevalov TV, Atuchin VV, et al. Optical properties of TiO$_2$ films deposited by reactive electron beam sputtering. J Elec Materi, 2017, 46: 6089–6095

30 Denton AR, Ashcroft NW. Vegard's law. Phys Rev A, 1991, 43: 3161–3164

31 Romano LT, Van de Walle CG, Ager III JW, et al. Effect of Si doping on strain, cracking, and microstructure in GaN thin films grown by metalorganic chemical vapor deposition. J Appl Phys, 2000, 87: 7745–7752

32 Ambacher O, Majewski J, Miskys C, et al. Pyroelectric properties of Al (In)GaN/GaN hetero- and quantum well structures. J Phys-Condens Matter, 2002, 14: 3399–3434

33 Dong L, Mantese JV, Avrutin V, et al. Strain induced variations in band

offsets and built-in electric fields in InGaN/GaN multiple quantum wells. J Appl Phys, 2013, 114: 043715

34 Li J, Li S, Kang J. Quantized level transitions and modification in In-GaN/GaN multiple quantum wells. Appl Phys Lett, 2008, 92: 101929

35 Dong L, Yadav SK, Ramprasad R, et al. Band gap tuning in GaN through equibiaxial in-plane strains. Appl Phys Lett, 2010, 96: 202106

36 Kueller V, Knauer A, Brunner F, et al. Growth of AlGaN and AlN on patterned AlN/sapphire templates. J Cryst Growth, 2011, 315: 200–203

37 Ni R, Chen X, Yan J, et al. Reducing stimulated emission threshold power density of AlGaN/AlN multiple quantum wells by nano-trench-patterned AlN template. J Alloys Compd, 2019, 777: 344–349

38 Li X, Xie H, Ponce FA, et al. Onset of surface stimulated emission at 260 nm from AlGaN multiple quantum wells. Appl Phys Lett, 2015, 107: 241109

39 Redwing JM, Loeber DAS, Anderson NG, et al. An optically pumped GaN-AlGaN vertical cavity surface emitting laser. Appl Phys Lett, 1996, 69: 1–3

40 Cosendey G, Castiglia A, Rossbach G, et al. Blue monolithic AlInN-based vertical cavity surface emitting laser diode on free-standing GaN substrate. Appl Phys Lett, 2012, 101: 151113

41 Feltin E, Christmann G, Dorsaz J, et al. Blue lasing at room temperature in an optically pumped lattice-matched AlInN/GaN vcsel structure. Electron Lett, 2007, 43: 924–926

42 Chyi J-I, Fujioka H, Morkoç H, et al. Development for ultraviolet vertical cavity surface emitting lasers. In: Proceedings Volume 9748, Gallium Nitride Materials and Devices XI. San Francisco, 2016

43 Liu YS, Saniul Haq AFM, Mehta K, et al. Optically pumped vertical-cavity surface-emitting laser at 374.9 nm with an electrically conducting n-type distributed Bragg reflector. Appl Phys Express, 2016, 9: 111002

44 Park YJ, Detchprohm T, Mehta K, et al. Optically pumped vertical-cavity surface-emitting lasers at 375 nm with air-gap/Al$_{0.05}$Ga$_{0.95}$N distributed Bragg reflectors. In: Proceedings of SPIE, Vertical-Cavity Surface-Emitting Lasers XXIII. San Francisco, 2019

45 Shen C, Leonard J, Young E, et al. GHz modulation bandwidth from single-longitudinal mode violet-blue VCSEL using nonpolar InGaN/GaN QWs. In: 2016 Conference on Lasers and Electro-Optics. San Jose, 2016

46 Ikeyama K, Kozuka Y, Matsui K, et al. Room-temperature continuous-wave operation of GaN-based vertical-cavity surface-emitting lasers with n-type conducting AlInN/GaN distributed Bragg reflectors. Appl Phys Express, 2016, 9: 102101

47 Furuta T, Matsui K, Kozuka Y, et al. 1.7-mW nitride-based vertical-cavity surface-emitting lasers using AlInN/GaN bottom DBRs. In: 2016 International Semiconductor Laser Conference (ISLC). Kobe, 2016

48 Matsui K, Kozuka Y, Ikeyama K, et al. Gan-based vertical cavity surface emitting lasers with periodic gain structures. Jpn J Appl Phys, 2016, 55: 05FJ08

49 Furuta T, Matsui K, Horikawa K, et al. Room-temperature CW operation of a nitride-based vertical-cavity surface-emitting laser using thick GaInN quantum wells. Jpn J Appl Phys, 2016, 55: 05FJ11

50 Chang TC, Kuo SY, Lian JT, et al. High-temperature operation of GaN-based vertical-cavity surface-emitting lasers. Appl Phys Express, 2017, 10: 112101

51 Lu TC, Chen SW, Wu TT, et al. Continuous wave operation of current injected GaN vertical cavity surface emitting lasers at room temperature. Appl Phys Lett, 2010, 97: 071114

52 Faraon A, Zhou W, Koyama F, et al. Gan vertical-cavity surface-emitting laser with a high-contrast grating reflector. In: Proceedings Volume 10542, High Contrast Metastructures VII. San Francisco, 2018

53 Higuchi Y, Omae K, Matsumura H, et al. Room-temperature CW lasing of a GaN-based vertical-cavity surface-emitting laser by current injection. Appl Phys Express, 2008, 1: 121102

54 Omae K, Higuchi Y, Nakagawa K, et al. Improvement in lasing characteristics of GaN-based vertical-cavity surface-emitting lasers fabricated using a GaN substrate. Appl Phys Express, 2009, 2: 052101

55 Terao K, Nagai H, Morita D, et al. Blue and green GaN-based vertical-cavity surface-emitting lasers with AlInN/GaN DBR. In: Proceedings of SPIE 11686, Gallium Nitride Materials and Devices XVI. Online only, 2021

56 Kasahara D, Morita D, Kosugi T, et al. Demonstration of blue and green GaN-based vertical-cavity surface-emitting lasers by current injection at room temperature. Appl Phys Express, 2011, 4: 072103

57 Chen R, Sun HD, Wang T, et al. Optically pumped ultraviolet lasing from nitride nanopillars at room temperature. Appl Phys Lett, 2010, 96: 241101

58 Yeh PS, Chang CC, Chen YT, et al. GaN-based vertical-cavity surface emitting lasers with sub-milliamp threshold and small divergence angle. Appl Phys Lett, 2016, 109: 241103

59 Park SH, Kim J, Jeon H, et al. Room-temperature GaN vertical-cavity surface-emitting laser operation in an extended cavity scheme. Appl Phys Lett, 2003, 83: 2121–2123

60 Izumi S, Fuutagawa N, Hamaguchi T, et al. Room-temperature continuous-wave operation of GaN-based vertical-cavity surface-emitting lasers fabricated using epitaxial lateral overgrowth. Appl Phys Express, 2015, 8: 062702

61 Hamaguchi T, Fuutagawa N, Izumi S, et al. Milliwatt-class GaN-based blue vertical-cavity surface-emitting lasers fabricated by epitaxial lateral overgrowth. Phys Status Solidi A, 2016, 213: 1170–1176

62 Hamaguchi T, Hoshina Y, Hayashi K, et al. Room-temperature continuous-wave operation of green vertical-cavity surface-emitting lasers with a curved mirror fabricated on {20−21} semi-polar GaN. Appl Phys Express, 2020, 13: 041002

63 Kuramoto M, Kobayashi S, Akagi T, et al. Enhancement of slope efficiency and output power in GaN-based vertical-cavity surface-emitting lasers with a SiO$_2$-buried lateral index guide. Appl Phys Lett, 2018, 112: 111104

64 Someya T, Werner R, Forchel A, et al. Room temperature lasing at blue wavelengths in gallium nitride microcavities. Science, 1999, 285: 1905–1906

65 Leonard JT, Cohen DA, Yonkee BP, et al. Nonpolar III-nitride vertical-cavity surface-emitting lasers incorporating an ion implanted aperture. Appl Phys Lett, 2015, 107: 011102

66 Holder CO, Leonard JT, Farrell RM, et al. Nonpolar III-nitride vertical-cavity surface emitting lasers with a polarization ratio of 100% fabricated using photoelectrochemical etching. Appl Phys Lett, 2014, 105: 031111

67 Leonard JT, Young EC, Yonkee BP, et al. Demonstration of a III-nitride vertical-cavity surface-emitting laser with a III-nitride tunnel junction intracavity contact. Appl Phys Lett, 2015, 107: 091105

68 Leonard JT, Yonkee BP, Cohen DA, et al. Nonpolar III-nitride vertical-cavity surface-emitting laser with a photoelectrochemically etched air-gap aperture. Appl Phys Lett, 2016, 108: 031111

69 Holder C, Speck JS, DenBaars SP, et al. Demonstration of nonpolar GaN-based vertical-cavity surface-emitting lasers. Appl Phys Express, 2012, 5: 092104

70 Mei Y, Yang TR, Ou W, et al. Low-threshold wavelength-tunable ultraviolet vertical-cavity surface-emitting lasers from 376 to 409 nm. Fundamental Res, 2021, 1: 684–690

71 Liu WJ, Hu XL, Ying LY, et al. Room temperature continuous wave lasing of electrically injected GaN-based vertical cavity surface emitting lasers. Appl Phys Lett, 2014, 104: 251116

72 Weng G, Mei Y, Liu J, et al. Low threshold continuous-wave lasing of yellow-green InGaN-QD vertical-cavity surface-emitting lasers. Opt Express, 2016, 24: 15546–15553

73 Zhang JY, Cai LE, Zhang BP, et al. Blue-violet lasing of optically pumped GaN-based vertical cavity surface-emitting laser with dielectric distributed Bragg reflectors. J Lightwave Technol, 2009, 27: 55–59

Author contributions Zheng Z fabricated the devices, measured the devices and epilayers, and wrote the manuscript. Hoo J grew the epitaxial structures and helped to measure the epilayers. Zhang B proposed the outline of the manuscript and revised the manuscript. Guo S helped to revise the manuscript. All the authors contributed to the discussion of the work.

Zhongming Zheng is a postdoctoral researcher at Xiamen University. He earned his PhD degree from Xiamen University in 2021. His research focuses on III-nitride materials and devices.

Shiping Guo received his PhD degree in semiconductor physics and device physics from Shanghai Institute of Technical Physics, Chinese Academy of Sciences, in 1994. Currently, he serves as Group Vice President and General Manager of MOCVD Product Division at AMEC. His research interests include MOCVD hardware development, project management and epitaxial growth process development of III-N based materials and devices. Before AMEC, he worked at IQR RF LLC and EMCORE Corp. from 2001 to 2012 and at several research groups at the City University of New York, Tohoku University and Shanghai Institute of Technical Physics.

Baoping Zhang was born in Hebei, China, in 1963. He received the BS degree in physics from Lanzhou University, Lanzhou, China, in 1983, the ME degree in microelectronics from Hebei Semiconductor Research Institute, Shijiazhuang, China, and the Dr. Eng. degree in applied physics from the University of Tokyo, Tokyo, Japan, in 1994. He is currently a distinguished professor at the School of Electronic Science and Engineering, Xiamen University, China, where he is engaged in wide-gap semiconductor materials and devices, especially GaN-based light-emitting diodes (LEDs) and VCSELs.

高质量的AlGaN外延结构和UVC垂直腔面发射激光器的实现

郑重明[1]，王玉坤[1]，胡建正[2]，郭世平[2*]，梅洋[1]，龙浩[1]，应磊莹[1]，郑志威[1]，张保平[1*]

摘要   AlGaN基垂直腔面发射激光器(VCSEL)因其优越的材料性质和器件优点吸引了很多关注. 然而, 由于材料外延生长和器件制备工艺的局限, AlGaN基VCSEL制备很困难. 本工作通过侧向外延生长技术制备了高质量的AlGaN多量子阱(MQWs)结构的外延片, 并通过X射线衍射(XRD)和光致发光(PL)实验对外延片进行了分析. XRD测量显示, 外延片中的AlN模板层几乎是弛豫的, 刃位错密度为10^9 cm^{-2}. 随后, 生长的AlGaN/AlN超晶格(SL)层被用来减少刃位错密度, 使得量子阱中的位错密度为10^8 cm^{-2}. 根据PL测试结果, MQWs的内量子效率(IQE)为62%, 且在室温下的发光以辐射复合为主. 通过激光剥离(LLO)和化学机械抛光(CMP)技术, 将这些外延片制备成UVC VCSEL. 经过这些工艺, MQWs的晶体质量没有受到影响, 还在抛光之后的表面观察到了UVC波段的受激辐射. 这些AlGaN基UVC VCSEL在275.91, 276.28和277.64 nm实现了激射, 最小激射阈值为0.79 MW cm^{-2}.